Accurate viscoelastic large deformation analysis using F-bar aided edge-based smoothed finite element method for 4-node tetrahedral meshes (F-barES-FEM-T4)

Yuki Onishi[1,a)], Ryoya Iida[1] and Kenji Amaya[1]

[1] Department of Systems and Control Engineering, Tokyo Institute of Technology, Japan

[a)]Corresponding and Presenting author: yonishi@a.sc.e.titech.ac.jp

ABSTRACT

A state-of-the-art tetrahedral smoothed finite element method, F-barES-FEM-T4, is demonstrated on viscoelastic large deformation problems. The stress relaxation of viscoelastic materials brings near incompressibility when the long-term Poisson's ratio is close to 0.5. The conventional hybrid 4-node tetrahedral (T4) elements cannot avoid the shear locking and pressure checkerboarding issues due to the incompressibility, meanwhile F-barES-FEM-T4 can suppress these issues successfully. A few examples of analyses verify that F-barES-FEM-T4 is locking-free and pressure oscillation-free in viscoelastic analyses as well as in nearly incompressible hyperelastic or elastoplastic analyses.

Keywords: Smoothed finite element method, Tetrahedral element, Large deformation, Viscoelasticity, Volumetric locking, Pressure checkerboarding.

Introduction

In a practical finite element solid analysis handling objects of arbitrary shapes, hexahedral mesh generation is impossible in many cases, and thus tetrahedral mesh generation is frequently used. However, the standard 1st-order 4-node tetrahedral (T4) elements cause the shear/volumetric locking, pressure checkerboarding, etc., which lead to low accuracy solutions. Although the standard 2nd-order 10-node tetrahedral elements avoid the shear locking, it does not improve the accuracy when the material have the incompressibility. In addition, it is well known that the volumetric locking and pressure checkerboarding issues are hardly improved even with finer meshes. Therefore, researching for high accuracy tetrahedral element development to handle material incompressibility is still being carried out actively.

The most popular method in high accuracy analysis with tetrahedral meshes is the hybrid elements based on the mixed variational principle. The standard displacement-based finite elements only have the nodal displacement as the unknown variables, whereas the hybrid elements additionally have the pressure and/or volumetric strain to avoid the volumetric locking and pressure checkerboarding. The 2nd-order 10-node tetrahedral hybrid element [2, 6] is known to have sufficient accuracy in relatively mild large deformation analysis and is widely used. However, this element has some disadvantages: reduced accuracy and convergence in severe large deformation analysis due to the influence of intermediate nodes; unavailability in dynamic explicit analysis due to the influence of hybrid formulation. The 1st-order 4-node tetrahedral hybrid element [2] is considered to be one of the current best options for severe large deformation analysis; yet, the shear locking issue, pressure checkerboarding issue, and disadvantages of hybridization have not been resolved. Some other advanced hybridization techniques for tetrahedral meshes [1, 15, 7] have been proposed but are still in research stage to date.

On the other hand, the smoothed finite element method (S-FEM) [5, 16, 9, 11] has recently attracted attention as a high accuracy analysis technique for tetrahedral meshes without using the mixed variational principle. S-FEM is a displacement-based finite element method that performs strain smoothing between adjacent elements and stress integration in smoothing domains around nodes, element edges or faces. Various S-FEM formulations have been proposed so far; in particular, the authors have proposed the F-bar aided edge-based S-FEM for T4 elements (F-barES-FEM-T4) [12] for high accuracy severe large deformation analysis. F-barES-FEM-T4 is a method that incorporates the F-bar method [3] into the tetrahedral edge-based S-FEM (ES-FEM-T4) so that it resolves the volumetric locking and pressure checkerboarding issues in nearly incompressible cases. The authors validated the effectiveness of F-barES-FEM-T4 for hyperelastic bodies (such as rubber materials) whose Poisson's ratio is close to 0.5 [12, 10, 14], and elastoplastic bodies (such as metal and plastic materials)

whose plasticity coefficient is much smaller than the elastic coefficient [13, 8]. It is thought that F-barES-FEM-T4 is equally effective for viscoelastic bodies (such as thermoplastic resin and glass materials) whose long-term Poisson's ratio is close to 0.5, but demonstration thereof has not yet been carried out.

In this paper, we apply F-barES-FEM-T4 to viscoelastic bodies with nearly incompressible long-term Poisson's ratio and demonstrate its performance in severe large deformation analysis. We handle a Hencky viscoelastic model based on the generalized Maxwell model described by a Prony series [4] and perform quasi-static analysis in which stress relaxation occurs. As the stress relaxation progresses, the incompressibility gradually increases; nevertheless, F-barES-FEM-T4 gives a highly accurate solution without locking or pressure checkerboarding. Analysis results of the conventional methods are also shown to demonstrate the effectiveness of F-barES-FEM-T4.

Methods

The method proposed in this paper is basically the same as F-barES-FEM-T4 [12, 10, 14, 13, 8] already proposed in the case of hyperelastic and elastoplastic body. The difference from the previous methods is only the calculation of the stress via material constitutive models and the state variables to be held. Therefore, in this paper, the calculation method of viscous strain and stress in the case of viscoelastic body is explained in detail, and the formulation of F-barES-FEM-T4 is described in brief. For details of F-barES-FEM-T4, please refer to the reference [12] etc..

Calculation of Deformation Gradient

Let us denote the deformation gradient at edge h in ES-FEM-T4 [5] by ${}^{\mathrm{Edge}}_{h}\widetilde{\boldsymbol{F}}$, then the isovolumetric part of the deformation gradient at edge h in F-barES-FEM-T4, ${}^{\mathrm{Edge}}_{h}\widetilde{\boldsymbol{F}}^{\mathrm{iso}}$, is described as

$$ {}^{\mathrm{Edge}}_{h}\widetilde{\boldsymbol{F}}^{\mathrm{iso}} = \left(\frac{1}{{}^{\mathrm{Edge}}_{h}\widetilde{J}} \right)^{1/3} {}^{\mathrm{Edge}}_{h}\widetilde{\boldsymbol{F}}; \tag{1} $$

$$ {}^{\mathrm{Edge}}_{h}\widetilde{J} = \det({}^{\mathrm{Edge}}_{h}\widetilde{\boldsymbol{F}}), \tag{2} $$

On the other hand, the volumetric part of the deformation gradient at edge h in F-barES-FEM-T4, ${}^{\mathrm{Edge}}\overline{\boldsymbol{F}}^{\mathrm{vol}}$, is given by the cyclic smoothing of J among elements and nodes followed by the edge-based smoothing (see reference [12] etc. for detail). Finally, the deformation gradient at edge h in F-barES-FEM-T4, ${}^{\mathrm{Edge}}_{h}\overline{\boldsymbol{F}}$, is obtained by combining ${}^{\mathrm{Edge}}_{h}\widetilde{\boldsymbol{F}}^{\mathrm{iso}}$ and ${}^{\mathrm{Edge}}\overline{\boldsymbol{F}}^{\mathrm{vol}}$ with the F-bar method.

$$ {}^{\mathrm{Edge}}_{h}\overline{\boldsymbol{F}} = {}^{\mathrm{Edge}}_{h}\overline{\boldsymbol{F}}^{\mathrm{vol}} \cdot {}^{\mathrm{Edge}}_{h}\widetilde{\boldsymbol{F}}^{\mathrm{iso}}. \tag{3} $$

The number of cyclic smoothing, c, is the tuning parameter of F-barES-FEM-T4. F-barES-FEM-T4 with c-time cyclic smoothings is referred to as "F-barES-FEM-T4(c)" hereafter in this paper.

Calculation of Stress

The Cauchy stress at edge h, ${}^{\mathrm{Edge}}_{h}\boldsymbol{T}$, is then derived in the standard way with ${}^{\mathrm{Edge}}_{h}\overline{\boldsymbol{F}}$. The following shows the derivation in case of the Hencky viscoelastic body based on the generalized Maxwell model described with the Prony series [4]. Hereafter in this subsection, ${}^{\mathrm{Edge}}_{h}\square$ is omitted.

The hydrostatic part of the Cauchy stress, $\boldsymbol{T}^{\mathrm{hyd}}$, is calculated in the same way as the Hencky hyperelastic body:

$$ \boldsymbol{T}^{\mathrm{hyd}} = K \, \mathrm{tr}(\boldsymbol{H}) \, \boldsymbol{I}, \tag{4} $$

where K is the bulk modulus (constant), $\mathrm{tr}(\square)$ is the operator to return the trace, and $\boldsymbol{H}$ is the Hencky (logarithmic) strain derived by ${}^{\mathrm{Edge}}\overline{\boldsymbol{F}}$. On the other hand, the deviatoric part of the Cauchy stress, $\boldsymbol{T}^{\mathrm{dev}}$, is given by

$$ \boldsymbol{T}^{\mathrm{dev}} = 2G_0 \left(\boldsymbol{H}^{\mathrm{dev}} - \sum_i g_i \boldsymbol{H}_i^{\mathrm{v}} \right), \tag{5} $$

where G_0 is the instantaneous shear modulus, g_i is the ith non-dimensional shear modulus in the Prony series, and $\boldsymbol{H}_i^{\mathrm{v}}$ is the ith Hencky (logarithmic) viscous strain. The logarithmic viscous strain after a time increment, $\boldsymbol{H}_i^{\mathrm{v}+}$, is calculated with the following time advancing equation.

$$ \boldsymbol{H}_i^{\mathrm{v}+} = \boldsymbol{R} \cdot \boldsymbol{H}_i^{\mathrm{v}} \cdot \boldsymbol{R}^T + \Delta \boldsymbol{H}_i^{\mathrm{v}}; \tag{6} $$

if $\Delta t \ll \tau_i$, then

$$\Delta \boldsymbol{H}_i^{\mathrm{v}} = \frac{\Delta t}{\tau_i}\left(\frac{1}{2}\Delta \boldsymbol{H}^{\mathrm{dev}} + \boldsymbol{R}\cdot(\boldsymbol{H}^{\mathrm{dev}} - \boldsymbol{H}_i^{\mathrm{v}})\cdot\boldsymbol{R}^T\right), \tag{7}$$

else

$$\Delta \boldsymbol{H}_i^{\mathrm{v}} = \left(1 - \frac{\tau_i}{\Delta t}\left(1 - \exp(-\frac{\Delta t}{\tau_i})\right)\right)\Delta \boldsymbol{H}^{\mathrm{dev}} + \left(1 - \exp(-\frac{\Delta t}{\tau_i})\right)\boldsymbol{R}\cdot(\boldsymbol{H}^{\mathrm{dev}} - \boldsymbol{H}_i^{\mathrm{v}})\cdot\boldsymbol{R}, \tag{8}$$

where Δt is the time increment, $\boldsymbol{R}$ is the rigid rotation in the time increment, and τ_i is the ith relaxation time in the Prony series. Conclusively, $\boldsymbol{T} = \boldsymbol{T}^{\mathrm{hyd}} + \boldsymbol{T}^{\mathrm{dev}}$ gives the Cauchy stress at each edge.

Calculation of Nodal Internal Force

The contribution of each edge to the nodal internal force, $\{{}^{\mathrm{Edge}}\boldsymbol{f}^{\mathrm{int}}\}$, is calculated in manner of the F-bar method:

$${}^{\mathrm{Edge}}_{h}f^{\mathrm{int}}_{P:p} = \frac{\partial {}^{\mathrm{Edge}}_{h}\widetilde{D}_{ij}}{\partial \dot{u}_{P:p}}\,{}^{\mathrm{Edge}}_{h}T_{pl}\,{}^{\mathrm{Edge}}_{h}V, \tag{9}$$

where ${}^{\mathrm{Edge}}\widetilde{\boldsymbol{D}}$ is the rate of stretching, u is the displacement, and V is the corresponding volume.

Results

Tensile Suspension of Viscoelastic Block

A large deformation analysis of a viscoelastic block subjected to horizontal tension and vertical gravity is performed. An outline of the analysis is shown in Fig. 1. The size of the block is $3 \times 2 \times 1$ m^3; its left end face is perfectly constrained; the right end face is quickly displaced 3 m in $+x$ direction for 10 s at a constant velocity and is kept the displacement for 1000 s so that the body is suspended. The material model is the Hencky viscoelastic body based on the generalized Maxwell model [4] with 1 MPa instantaneous Young's modulus, 0.3 instantaneous Poisson ratio, 0.96 non-dimensional shear modulus for the 1st (and only) term of the Prony series (i.e., the long-term Young's modulus is about 0.046 MPa and the long-term Poisson's ratio is about 0.49) and its relaxation time constant is 10 s. The mass density is 1000 kg / m^3, and the gravitational acceleration is 9.8 m/s^2 in $-z$ direction. An unstructured 4-node tetrahedral mesh with 0.2 m seed size (1405 nodes and 6183 elements) is prepared and is analyzed by F-barES-FEM-T4(c) for $c = 1, 2, 3$ and also by the conventional 4-node tetrahedral element (ABAQUS C3D4) and its hybrid element (ABAQUS C3D4H). In addition, an analysis is also performed with the 8-node hexahedral selective reduced integration element (ABAQUS C3D8) using a structured mesh in the same seed size (1122 nodes and 800 elements) as a reference solution.

Figure. 2–5 show the deformations and stress distributions of the analysis results. Since the viscoelastic body at the initial stage of analysis shows behavior close to a compressible elastic body with the instantaneous modulus, relatively minor errors are only observed in the results at the end of the tension ($t = 10$ s). However, since it shifts to behavior close to an incompressible elastic body with the long-term modulus over time, relatively major errors are observed in the results at the end of the analysis ($t = 1010$ s). ABAQUS C3D4 clearly suffered from shear/volumetric locking and pressure checkerboarding. Although ABAQUS C3D4H shows a relatively smooth Mises stress distribution, it can be seen that the pressure distribution is partly in the checkerboard pattern. On the other hand, every F-barES-FEM-T4 shows smooth distributions not only in the Mises stress but also in the pressure.

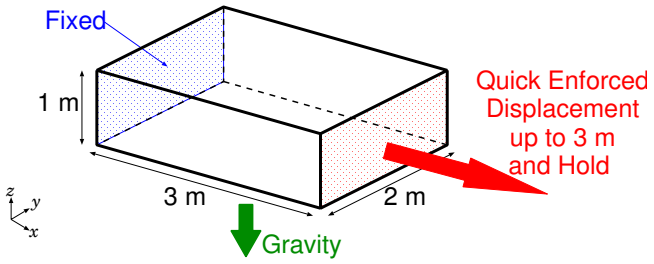

Figure 1. Outline of the tensile suspension analysis of a viscoelastic block.

Figure. 6 compares the displacement time histories of the node at the center of the bottom face in z direction. The node is displaced in $+z$ direction up to 10 s because of the decrease in the cross-sectional area due to the quick tension of the block in a compressible state. Meanwhile, the node hangs down in $-z$ direction after 10 s because of the stress relaxation and gravity and approaches to the long-term stable position gradually. Because ABAQUS C3D4 can not avoid both shear and volumetric locking, a much harder solution is obtained. Although ABAQUS C3D4H avoids volumetric locking, sheer locking can not be avoided [12] and thus a slightly hard solution is obtained. On the other hand, F-barES-FEM-T4s show the almost same accuracy solutions as ABAQUS C3D8 regardless of the number of cyclic smoothings c, which confirms that our method avoids both shear and volumetric locking.

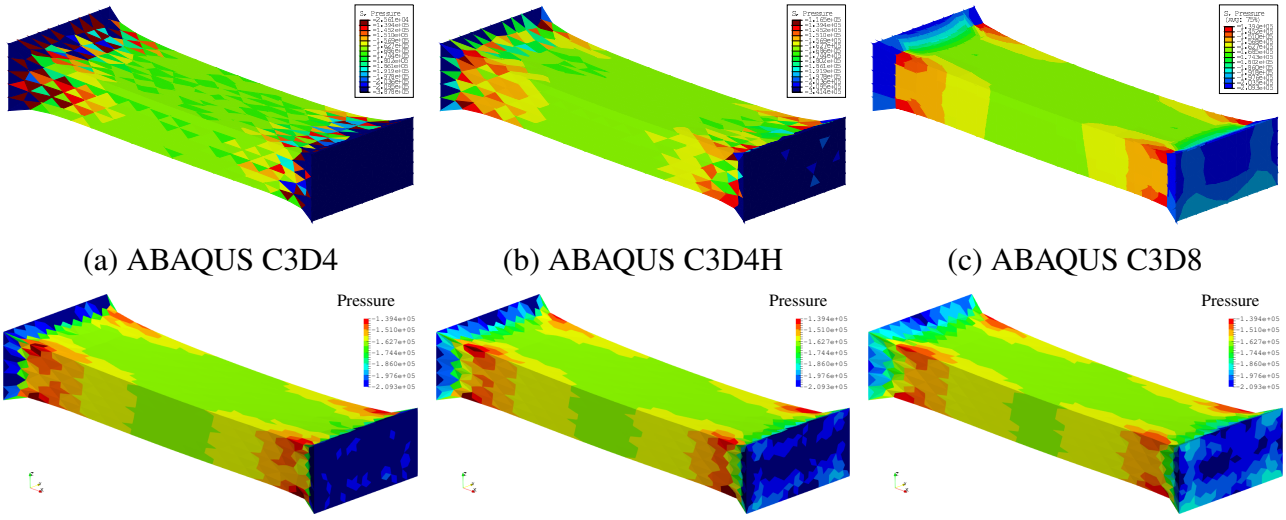

(a) ABAQUS C3D4 (b) ABAQUS C3D4H (c) ABAQUS C3D8

(d) F-barES-FEM-T4(1) (e) F-barES-FEM-T4(2) (f) F-barES-FEM-T4(3)

Figure 2. Comparison of pressure distributions at the end of the tension (t = 10 s) in the tensile suspension analysis. The contour range is [−209.3 kPa, −139.4 kPa] and is in common with each other.

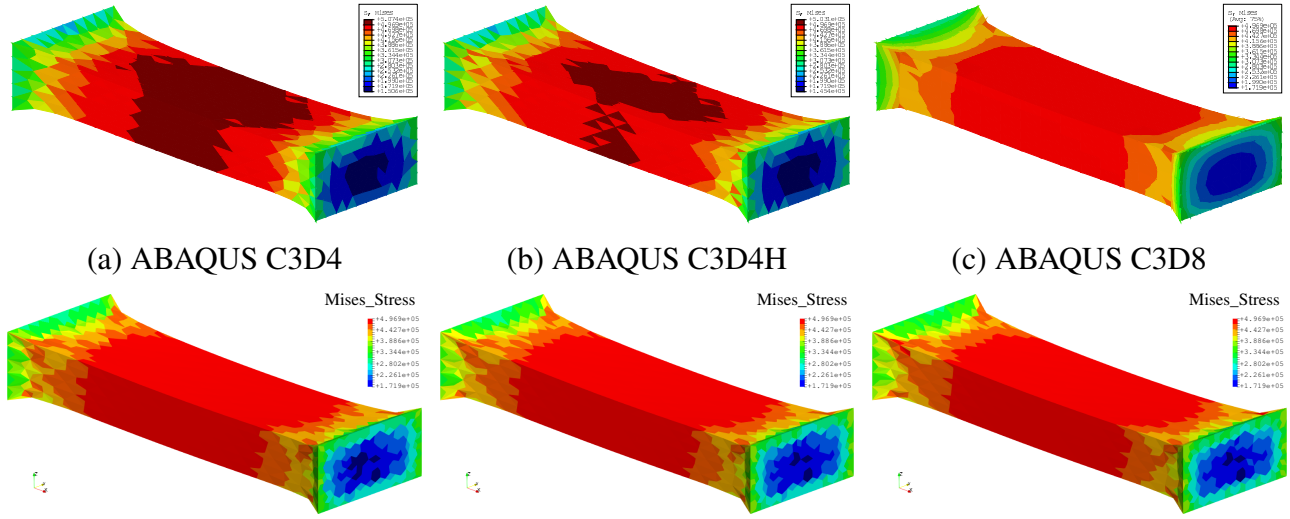

(a) ABAQUS C3D4 (b) ABAQUS C3D4H (c) ABAQUS C3D8

(d) F-barES-FEM-T4(1) (e) F-barES-FEM-T4(2) (f) F-barES-FEM-T4(3)

Figure 3. Comparison of Mises stress distributions at the end of the tension (t = 10 s) in the tensile suspension analysis. The contour range is [171.9 kPa, 496.9 kPa] and is in common with each other.

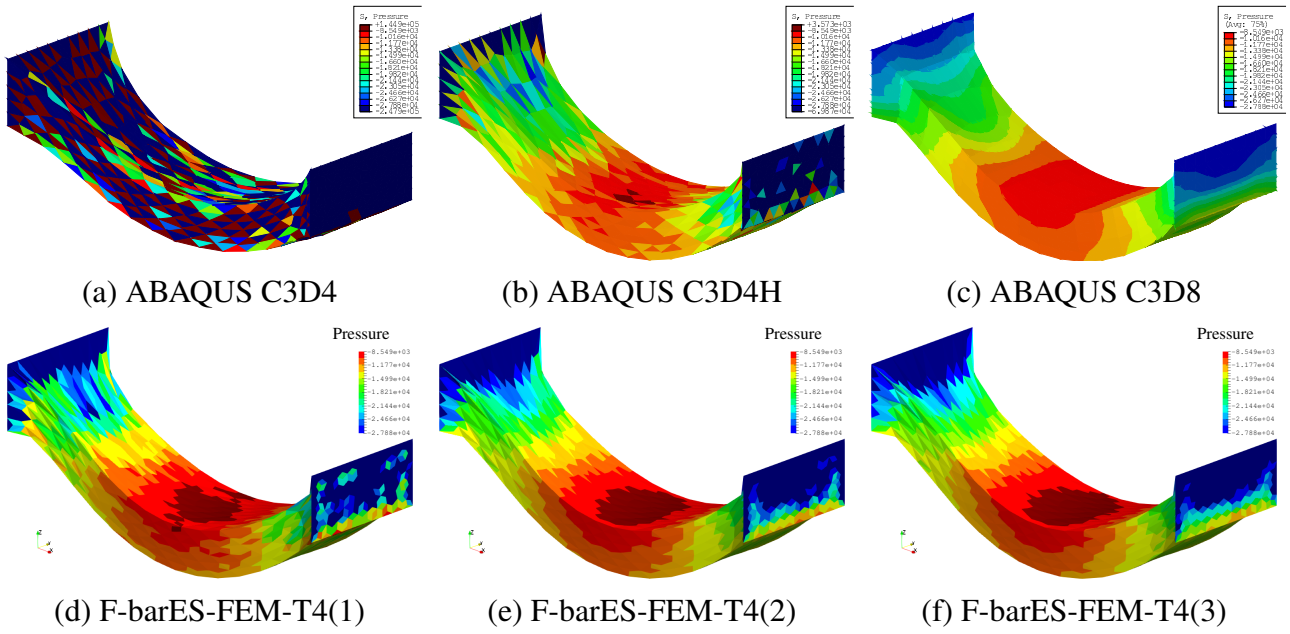

(a) ABAQUS C3D4 (b) ABAQUS C3D4H (c) ABAQUS C3D8

(d) F-barES-FEM-T4(1) (e) F-barES-FEM-T4(2) (f) F-barES-FEM-T4(3)

Figure 4. Comparison of pressure distributions at the end of the analysis ($t = 1010$ s) in the tensile suspension analysis. The contour range is [-27.88 kPa, -8.549 kPa] and is in common with each other.

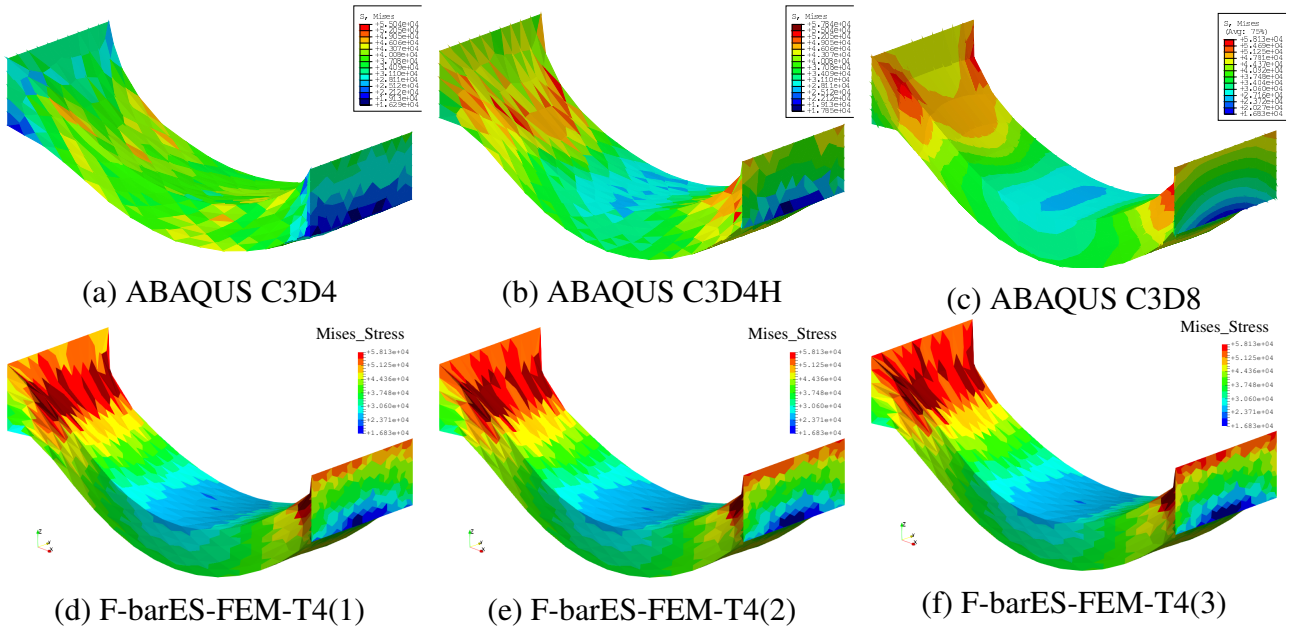

(a) ABAQUS C3D4 (b) ABAQUS C3D4H (c) ABAQUS C3D8

(d) F-barES-FEM-T4(1) (e) F-barES-FEM-T4(2) (f) F-barES-FEM-T4(3)

Figure 5. Comparison of Mises stress distributions at the end of the analysis ($t = 1010$ s) in the tensile suspension analysis. The contour range is [16.83 kPa, 58.13 kPa] and is in common with each other.

Tensile Drooping of Viscoelastic Twisted Prism

A large deformation analysis of a viscoelastic twisted prism subjected to vertical tension and gravity is performed. An outline of the analysis is shown in Fig. 7. The body to be analyzed is an object whose height is 10 m and whose cross-section is a right triangle with 3, 4, and 5 m side lengths twisted 180 degrees around the center of cross-sections, which is difficult to be meshed into regular hexahedral elements. The bottom face is perfectly constrained; the top face is quickly displaced 5 m in $+z$ direction for 10 s at a constant velocity and is kept the displacement for 1500 s so that the body is drooped. The material model is almost the same as the previous example, except that the instantaneous Young's modulus

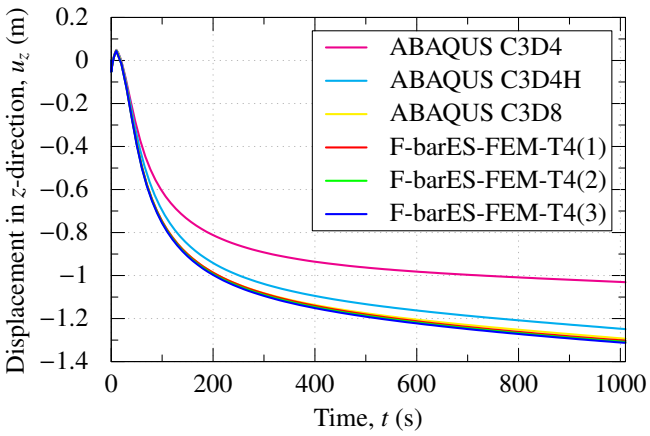

Figure 6. Comparison of displacement time histories of the node at the center of the bottom face in z direction in the tensile suspension analysis.

is 2 MPa. An unstructured 4-node tetrahedral mesh with 0.5 m seed size (960 nodes and 3514 elements) is prepared and is analyzed by F-barES-FEM-T4(2) and ABAQUS C3D4H.

Figure 8–10 compare the deformations and pressure distributions of the analysis results. As in the previous example, there are only minor differences between F-barES-FEM-T4(2) and ABAQUS C3D4H at an earlier stage (t = 10 s) although a little pressure oscillations are observed in the result of ABAQUS C3D4H. However, there are major difference between them at an later stage (t = 1510 s), where a sufficient time has passed compared to the relaxation time constant. The pressure sign distribution of ABAQUS C3D4H shows clear pressure checkerboarding and thus its stress distribution must be inaccurate. Also, the drooping deformation of ABAQUS C3D4H is slightly smaller than that of F-barES-FEM-T4(2), which is probably because of the tendency of ABAQUS C3D4H giving a harder solution. Since F-barES-FEM-T4(2) shows the pressure distributions without any oscillation, it seems to give a more appropriate displacement/stress solution.

Conclusion

A state-of-the-art tetrahedral smoothed finite element method, F-barES-FEM-T4, was demonstrated in quasi-static viscoelastic large deformation analyses. Comparison with the conventional hybrid tetrahedral element (ABAQUS C3D4H) applicable to severe large deformation problems, the proposed method was locking-free and pressure checkerboarding-free and thus gave far better solutions in displacement and stress as well as hyperelastic and elastoplastic cases with material incompressibility. When analyzing the relaxation behavior for a time sufficiently longer than the relaxation time

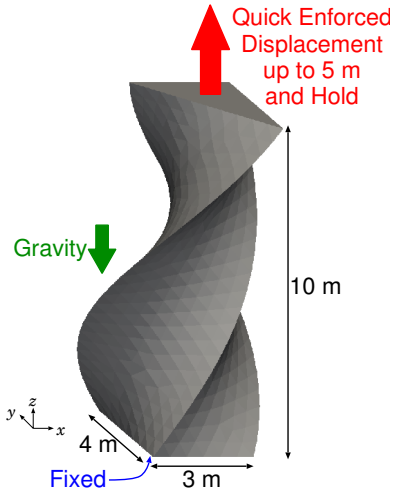

Figure 7. Outline of the tensile drooping analysis of a viscoelastic twisted prism.

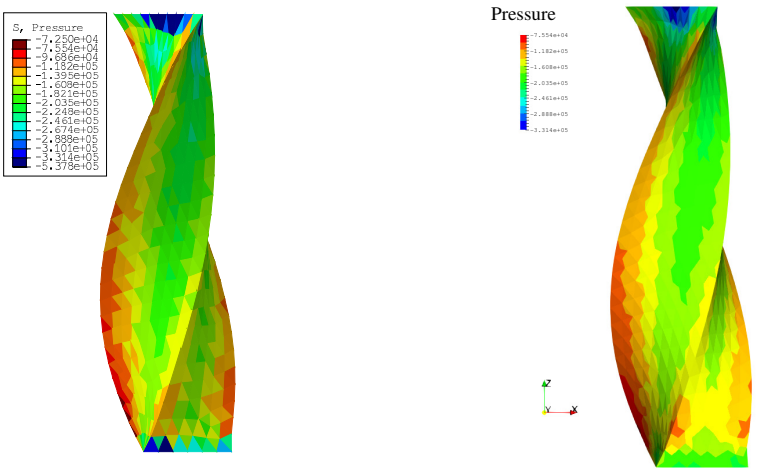

(a) ABAQUS C3D4H (b) F-barES-FEM-T4(2)

Figure 8. Comparison of pressure distributions at the end of the tension (t = 10 s) in the tensile drooping analysis. The contour range is [−331.4 kPa, −75.54 kPa] and is in common.

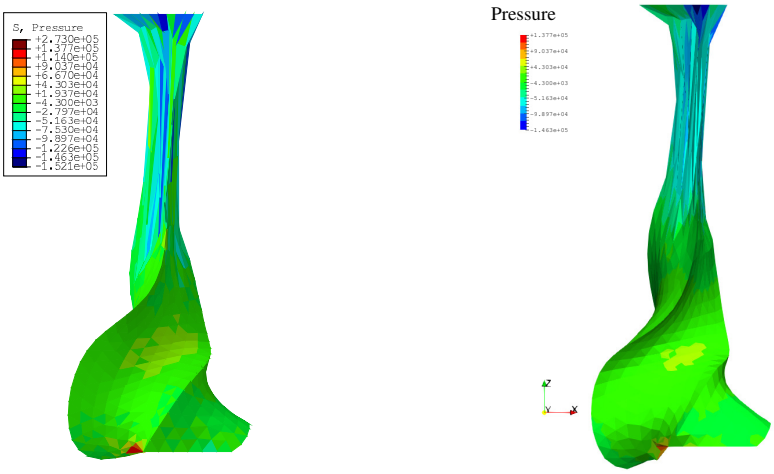

(a) ABAQUS C3D4H (b) F-barES-FEM-T4(2)

Figure 9. Comparison of pressure distributions at the end of the analysis (t = 1510 s) in the tensile drooping analysis. The contour range is [−146.3 kPa, +137.7 kPa] and is in common.

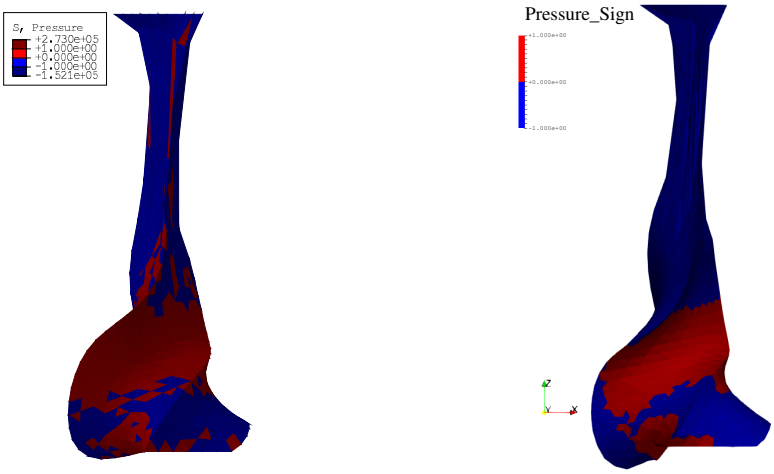

(a) ABAQUS C3D4H (b) F-barES-FEM-T4(2)

Figure 10. Comparison of pressure sign distributions at the end of the analysis (t = 1510 s) in the tensile drooping analysis. The red and blue colors represent the compressed and tensile parts, respectively.

with respect to the viscoelastic material, it is inevitable to treat the near incompressibility because the long-term material constants decide the phenomenon. Therefore, the proposed method is thought to be effective for resin molding simulations in complex shapes around the glass transition temperature.

F-barES-FEM-T4 is one of the best tetrahedral FE formulations superior in all rubbers, plastic metals and viscoelastic resins in which incompressibility appears. A wide practical use of F-barES-FEM-T4 for more complex body shapes is expected in the future.

References

[1] Bonet, J., Gil, A. J., Lee, C. H., Aguirre, M., and Ortigosa, R. (2015). A first order hyperbolic framework for large strain computational solid dynamics. part i: Total lagrangian isothermal elasticity. *Computer Methods in Applied Mechanics and Engineering*, 283:689 – 732.

[2] Corp., D. S. S. (2013). *ABAQUS 6.13 Theory Guide*. Dassault Systèmes Simulia Corp., Providence, RI, USA.

[3] de Souza Neto, E., Peric, D., Dutko, M., and Owen, D. (1996). Design of simple low order finite elements for large strain analysis of nearly incompressible solids. *International Journal of Solids and Structures*, 33(20-22):3277–3296.

[4] de Souza Neto, E. A., Peric, D., and Owen, D. R. J. (2008). *Computational Methods for Plasticity: Theory and Applications*. Wiley, Hoboken, NJ, USA.

[5] Liu, G. R. and Nguyen-Thoi, T. (2010). *Smoothed Finite Element Methods*. CRC Press, Boca Raton, FL, USA.

[6] MSC Software Corp. (2013). *MARC 2013.1 Volume A: Theory and User Information*. MSC Software Corp., Santa Ana, CA, USA.

[7] Ong, T. H., Heaney, C. E., Lee, C.-K., Liu, G., and Nguyen-Xuan, H. (2015). On stability, convergence and accuracy of bES-FEM and bFS-FEM for nearly incompressible elasticity. *Computer Methods in Applied Mechanics and Engineering*, 285(0):315–345.

[8] Onishi, Y. (2017). F-bar aided edge-based smoothed finite element method with 4-node tetrahedral elements for static large deformation elastoplastic problems. *International Journal of Computational Methods*, under review.

[9] Onishi, Y. and Amaya, K. (2014). A locking-free selective smoothed finite element method using tetrahedral and triangular elements with adaptive mesh rezoning for large deformation problems. *International Journal for Numerical Methods in Engineering*, 99(5):354–371.

[10] Onishi, Y. and Amaya, K. (2015a). F-bar aided edge-based smoothed finite element method with tetrahedral elements for large deformation analysis of nearly incompressible materials. *The 6th International Conference on Computational Methods (ICCM2015)*.

[11] Onishi, Y. and Amaya, K. (2015b). Performance evaluation of the selective smoothed finite element methods using tetrahedral elements with deviatoric/hydrostatic split in large deformation analysis. *Theoretical and Applied Mechanics Japan*, 63:55–65.

[12] Onishi, Y., Iida, R., and Amaya, K. (2017). F-bar aided edge-based smoothed finite element method using tetrahedral elements for finite deformation analysisof nearly incompressible solids. *International Journal for Numerical Methods in Engineering*, 109(11):1582–1606.

[13] Onishi, Y., Ryoya, I., and Amaya, K. (2016). F-bar aided edge-based smoothed finite element methods with 4-node tetrahedral elements for static large deformation hyperelastic and elastoplastic problems. *The 7th International Conference on Computational Methods (ICCM2016)*.

[14] Ryoya, I., Onishi, Y., and Amaya, K. (2016). Performance evaluation of various smoothed finite element methods with tetrahedral elements in large deformation dynamic analysis. *The 7th International Conference on Computational Methods (ICCM2016)*.

[15] Scovazzi, G., Carnes, B., Zeng, X., and Rossi, S. (2016). A simple, stable, and accurate linear tetrahedral finite element for transient, nearly, and fully incompressible solid dynamics: a dynamic variational multiscale approach. *International Journal for Numerical Methods in Engineering*, 106(10):799–839. nme.5138.

[16] Zeng, W. and Liu, G. R. (2016). Smoothed finite element methods (S-FEM): An overview and recent developments. *Archives of Computational Methods in Engineering*, pages 1–39.